Influence of strain-rate on the interaction between towed fishing gears and the seabed

Shamendra Malinga Aluwihare[1], Ana Ivanović[1]* and Finbarr G O'Neill[2]

[1]School of Engineering, University of Aberdeen, AB24 3UE, Aberdeen, Scotland, UK

[2]Technical University of Denmark, National Institute of Aquatic Resources, (DTU Aqua), Willemoesvej 2, 9850 Hirtshals, Denmark

Abstract

The ability to predict the seabed penetration and the drag force of the gear components of demersal trawlers is of significant benefit to the fisheries industry. It allows for the design of gears of reduced environmental impact and of improved fuel efficiency. This study presents a single-phase strain rate dependent soil model that can accurately predict deformation of a saturated granular soil. Elements of an otter trawl system are modelled as simplified discs which are then translated across a seabed at given speed where horizontal drag force and vertical penetration is measured. This is facilitated using an explicit Finite Element (FE) model developed in ABAQUS alongside a Coupled Eulerian-Lagrangian (CEL) mesh. Comparisons against laboratory experiments showed that the model was correctly able to capture the increase in drag force with towing speed. Further comparisons against full scale sea trials indicated the model generally compared well against test data and correctly identified the trends and magnitudes of drag force against towing speed. From these results, the influence of strain rate in the soil was studied in detail and conclusions drawn on the resultant drag force and penetration of towed fishing gears on the seabed.

1. Introduction

Towed demersal fisheries are a vital constituent of the global fishing industry and account for up to 23% of catch worldwide [1]. There are many variants of demersal towed fishing gears and their specific design depends on the species being targeted, the vessels used, the economic resources of the fishers and historical practices and traditions [1]. In general, they comprise a net that is weighted to maintain contact with the seabed and that is kept open by floats. Otter trawls are one of the most common types of demersal fishing gear (Figure 1). With this method of trawling, the otter doors, sweeps, bridles and ground gear are in contact with the seabed while the floats are used keep the upper extremity of the net buoyant, maintaining the opening of the net. In their simplest form, demersal otter doors can be described as low aspect ratio rectangles while the other elements can be described as discs of low and high aspect ratios. The physical impact of otter trawls can have ecological and environmental consequences. There can be significant penetration into the seabed leading to benthic mortality, release of nutrients, alterations to the biogeochemistry and habitat destruction. Hence, to ensure that fisheries are managed in a biologically sustainable and an economically viable manner, there is a need for a better understanding of the geotechnical contact between the trawl gear and the seabed and the resulting penetration and deformation of the soil stratum.

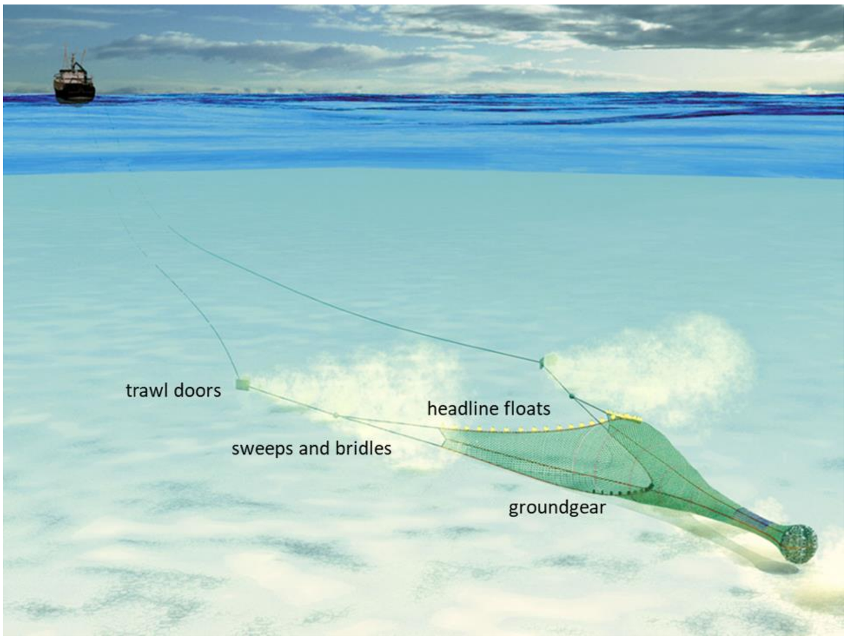

Figure 1: Otter Trawling Gear [3]

While studies have been conducted gathering data on the retrospective effects of trawling on the seabed [4] [5] [6] [7] [8] [9], much less has been done to develop predictive models to describe this. The use of FE methods to model the soil structure interaction caused by towed fishing gears typically poses two fundamental problems; (i) the large deformations associated with soil and (ii) the effect of pore pressure which affects shear strength of soil. Qiu et al. [10] describes the use of explicit Coupled Euler Lagrangian (CEL) methods to solve geotechnical problems involving large deformations. It has been used by Hamann et al. [11], to simulate pile jacking, and Van den Abeele et al. [12] to study soil deformations observed during pipeline embedment and berm formation. Yi et al [13] employed a material subroutine to describe the evolution of pore pressure within granular soils with a single-phase approximation. Dutta [14] and Dutta et al [15] studied the use of CEL mesh with Abaqus/Explicit to simulate pipeline embedment in to the seabed, where they adopted a single-phase strain-rate dependent constitutive soil model based on observations by Zhou and Randolph [16]. Hambleton and Drescher [17], presented a case for the FE analysis of a non-driven disc moving through a frictional and cohesive soils using an arbitrary Lagrangian/Eulerian mesh. This work also studied the use of analytical models and highlighted the limitations of such models. Ivanovic et al [18] and Esmaeili and Ivanović [19] [20] have studied the application of an explicit FE solver to model the interaction between discs (of thickness, t and diameter, d) and a sandy seabed. These efforts illustrated the formation of a frontal berm (of height b as shown in Figure 2) in front of towed discs and demonstrated that the total geotechnical drag they experienced was a combination of frictional forces and passive pressure caused by the berm formation. Esmaeili and Ivanović [19] [20] also demonstrated the effect of varying the angle of attack (angle of the geometry relative to direction of motion) on a rockhopper assembly.

The effect on strain rate on a partially embedded object translating across the seabed is predicated on the work done by Palmer [21] ,van Os & van Leussen [22] and Lauder et al [23] [24]. Observations from these studies demonstrated that during high strain-rate deformations, the soil exhibits a partially drained response. This is a result of the dilation of the soil under shear, which then affects the flow of the pore water across the pressure gradient created. If the rate of deformation is greater than the time taken for this gradient to equalise, the total stress transmitted back is a result of the instantaneous pore water pressure and the resistance provided by the soil skeleton. This is not an unlimited increase however, as at higher strain-rates, the soil produces a fully undrained response within the shear zone as a maximum negative pore pressure is reached. This rate effect is dependent on the permeability, dilation and void ratio of the granular soil being studied.

Experimental measurements of the rate-effect in saturated soils have been undertaken in previous studies [25] [26] [27] [28] [29] [30] and have broadly concluded that an increase of friction angle of the soil can be observed with increasing rates of deformation. In this paper, this type of rate-dependant shear strength is coupled to a constitutive soil model in a Finite Element (FE) solver as described by Aluwihare [31] to simulate the change in shear strength of the soil with strain rate. The resultant effect on towed fishing gears and the mechanics of the interaction of non-rolling discs with saturated sandy soils under a range of dimensions, weights, and speeds is examined. Non-rolling discs were chosen specifically as they are representative of the clump weights, ropes and rockhopper groundgears that are found in demersal trawl gear and which are responsible for a large proportion of the seabed contact [18].

More specifically, a disc of diameter *d* and weight *W* moving at speed *s* and causing a vertical seabed penetration *z*, is investigated. This results in the formation of a frontal berm of height *b* and causes a resistance to motion in the form of a drag force F_D. (Figure 2, Table 1). By making comparisons with experimental data, it is demonstrated that the resulting FE model provides an accurate description of non-rolling discs interacting with sandy soils. Non-rolling discs are an integral part of many fishing gear components that are in contact with the seabed and hence this model will help provide a better understanding of the physical impact of these gears on benthic habitats.

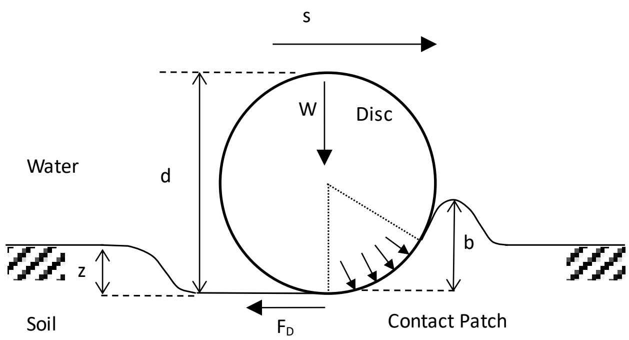

Figure 2: Schematic of non-rolling disc on soil

Table 1: Table of symbols

Parameter	Symbol	Unit
Area	A	m^2
Diameter	d	m
Horizontal Drag Force	F_D	N
Geometry Weight	W	N
Number of Discs	n	m
Soil Unit Weight	γ	Nm^{-3}
Strain rate	$\dot{\varepsilon}$	s^{-1}
Thickness	t	m
Towing Speed	s	ms^{-1}
Unit Displacement in Abaqus	U	-
Unit Rotation in Abaqus	UR	-
Vertical Penetration	z	m

2. Numerical Modelling

2.1. FE Model Description

The numerical modelling carried out in this study is based on the methodology described by Aluwihare [31]. This methodology used the ABAQUS/Explicit finite element package with a Coupled Eulerian-Lagrangian (CEL) meshing technique. CEL mesh uses a combination of Lagrangian mesh elements, where element coordinates are time invariant and move with the material when the body undergoes deformation, and Eulerian elements, where element coordinates are spatially fixed and allow the movement of material through them. Using both mesh techniques in the same model minimises the mesh dependency exhibited by a traditional Lagrangian mesh when undergoing large deformations [20] [32] [33].

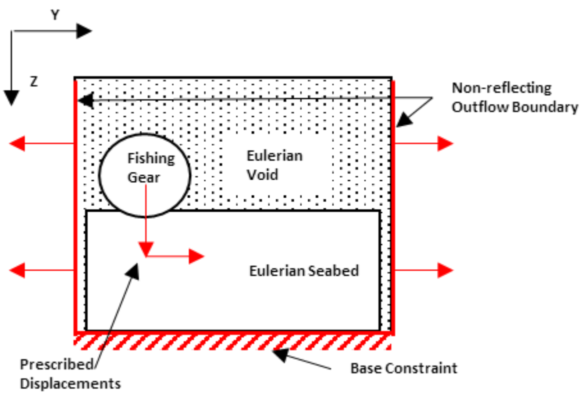

Figure 3: FE Model set-up

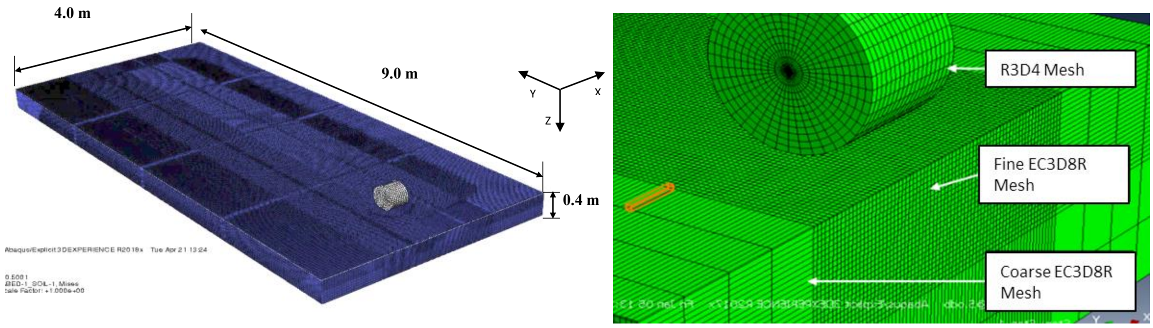

(a) (b)

Figure 4: Example FE model for single disc geometry (a) with zoomed in section showing local mesh refinement (b)

The reference configuration of the FE model is shown in Figure 3. The FE Model assumes a perfectly flat, saturated granular seabed. The simulation mesh consisted of 1.6E+06 Eulerian

8-noded 3D brick elements (EC3D8R) to discretize the seabed as shown in Figure 4 (a), while the disc was modelled as a rigid body with 8.2E+02 4-node elements (R3D4) as shown in Figure 4 (b). A sensitivity analysis was carried out on mesh sizing to eliminate any influence on mesh size on the results which led to the selected mesh elements. A partitioned meshing strategy was subsequently adopted to reduce computational time. The simulation consisted of two dynamic steps; (i) to allow penetration due to weight of the disc ($\ddot{U}Z \neq 0$) and (ii) to impose a horizontal velocity ($\dot{U}Y \neq 0$) on the disc while $UZ \neq 0$ and all other Degrees of Freedom remain constrained.

2.2. Constitutive Soil Models

To develop a material model for soil, it is first important to understand the impact of the solid skeleton and the pore fluid pressure on the applied stress. Terzaghi [34], proposed the principal of effective stress to describe the relationship between effective stress, σ', total stress, σ and pore fluid pressure, u, where $\sigma = \sigma' + u$ [35].

2.2.1. Drucker-Prager Constitutive Model

For the purposes of this study, the Drucker-Prager (DP) model was chosen as it natively supports strain-rate dependant yield stress. The DP model is used commonly within soil mechanics as it can model pressure dependant yield while assuming elasto-plastic behaviour. This can be expressed in terms of invariants of a stress tensor as [36]:

$$F = S_{DP} - p \tan \beta - c_{DP} = 0 \quad (1)$$

Where β is the friction angle of the material on the *p-t* plane, c_{DP} is the cohesion measured on the same, p is the first invariant of general stress and S_{DP} is deviatoric stress measure. The DP model also follows the non-associated flow rule for the plastic flow potential ($\phi \neq \psi$). Within Abaqus/Explicit, the shear strength of the soil is coupled to the strain rate using the parameter $\bar{\sigma}$, which in this case is equal to the cohesion yield stress, c_{DP}, and can be expressed in terms of strain-rate as follows:

$$\bar{\sigma} = c_{DP} = R\sigma^0 \quad (2)$$

Where σ^0 is the yield stress at a static state ($\sigma^0 = c_{DP}$) and $R(\dot{\bar{\varepsilon}}^{pl})$ is a function of strain rate ($R=1.0$ at $\dot{\bar{\varepsilon}}^{pl}=0$) which scales yield stress based on the strain-rate [36]. The properties for the DP model used in this study were based on triaxial compression and shear box testing performed previously and are summarised in

Table 2 [20] [37].

Table 2: Constitutive model parameters [37] [38]

Parameter	Value	Unit
Critical Friction Angle, ϕ' (β)	32 (43)	°
Dilation Angle, ψ	0.1	°
Young's Modulus, *E*	8	MPa
Poisson's Ratio, *v*	0.3	-
d_{50}	0.17	mm
d_{10}	0.13	mm
Specific Weight (wet), γ	22400	Nm^{-3}
$\dot{\varepsilon}_{limit}$	10	-
Permeability, *k*	5.0E-4	ms^{-1}

2.3. Modelling Strain-Rate Dependency in Saturated Granular Soils

The relationship between strain rate and the shear strength of soil, investigated and quantified by Watanabe et al [30], has been applied to this study as described in Aluwihare [31]. The proposed approach involved approximating the change in shear strength of the soil under shear using a single-phase model natively available in FEA packages, avoiding the limitations typically imposed by two-phase models. By coupling strain rate of the soil undergoing shear to an increase in effective stress, the fluid phase could be neglected from the model. Under low strain rates the model would present as a drained soil. Experimental observations from [30] allowed the effective friction angle of soil to be plotted against strain rate as shown in Figure 5. Where ϕ'/ϕ'_{ref} is the ratio between the effective friction angle, ϕ' and the reference effective friction angle ϕ'_{ref}. The DP model in Abaqus/Explicit offers a native ability to couple strain rate and shear strength. However, this cannot resolve the increase in friction angle, but instead scales cohesion based on strain rate. By scaling cohesion between the minimum and maximum strain rates, the increase in shear strength of the soil was simulated in the area of the soil undergoing shear, allowing for the FE model to more accurately replicate saturated soil interacting with the towed discs.

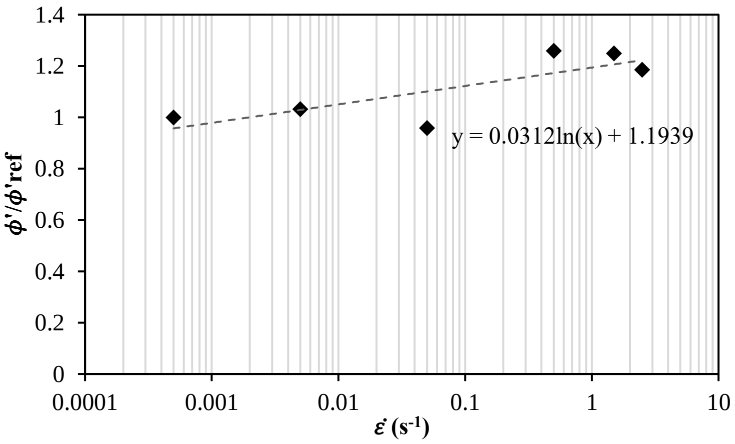

Figure 5: Increase in friction angle with strain rate

Watanabe et al [30] concluded that while $\dot{\varepsilon} < 0.005\ s^{-1}$ there was no change in shear strength as fully drained conditions persisted. While $\dot{\varepsilon} > 0.005\ s^{-1}$ an increase in shear strength was seen due to partial drainage. This increase was also postulated to reach a maximum when the soils would become fully undrained. Due to experimental limitations this maximum was determined to be above $\dot{\varepsilon} > 2.5\ s^{-1}$. This study considered the increase in strength to reach a maximum at $\dot{\varepsilon} = 10\ s^{-1}$ for simulation purposes [31] as this was the maximum strain rate induced in the soil.

3. Validation of FE Model

To validate the numerical model, comparisons were made against existing experimental observations under laboratory [37] (Figure 7) and field conditions [9] (

Figure 10). The geometries studied consisted of non-rolling truncated discs of varying sizes and weights (Figure 6 and Table 3) and are separated into single disc and multiple disc geometries.

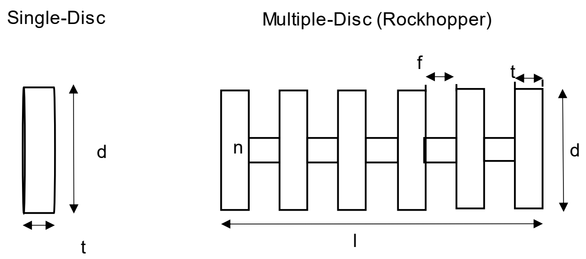

Figure 6: Schematic diagram of geometries modelled

The properties of penetration, drag force and weight are expressed using non-dimensional terms which are developed using a unique soil property (unit weight) and geometry dimensions as shown in Hambleton and Drescher [17]. The expression for speed is obtained by first obtaining strain rate as a function of speed and the diameter of the given geometry. The non-dimensional expression is then obtained as a function of strain rate and the limiting strain rate of the soil as described in Section 2.3. It is noted that this expression still maintains a linear relationship with speed.

The following non-dimensional parameters are used to present results:

$$\bar{z} = \frac{z}{d} \quad \bar{F} = \frac{F_D}{\gamma t d^2} \quad \bar{W} = \frac{W}{\gamma t d^2} \quad \dot{\varepsilon} = \frac{s}{d} \quad \bar{\varepsilon} = \frac{\dot{\varepsilon}}{\dot{\varepsilon}_{limit}}$$

Table 3: Loadcase matrix for comparison against experimental results

Type	Diameter d (m)	Thickness t (m)	Spacing f (m)	Length l (m)	Area A (m^2)	Speed s (ms^{-1})	Weight W (N)
Single Disc	0.12	0.09	-	-	0.011	0.01-0.21	- (fixed z)
Single Disc	0.20	0.15	-	-	0.03	1.2,1.5, 1.8	576, 1176, 1764
Multiple Disc (Rockhopper)	0.20	0.025	0.075	0.525	0.03		

3.1. Validation with Laboratory Experiments

The FE model was compared against laboratory experiments conducted by Casanovas-Revilla [37]. These experiments were used to determine the horizontal drag force experienced by a single disc being actuated across a saturated sand channel at a fixed penetration. The laboratory experiments were performed using a rigid disc attached to a mobile trolley which was then actuated along a sand channel as shown in Figure 7. The trolley was actuated using a pulling wire attached to a motor. A loadcell contained within the trolley allowed for horizontal drag force to be measured. The experiments used a fixed vertical penetration (z=0.009m, $\bar{z}$ = 0.075) which allowed the effect of varying $\bar{z}$ on $\bar{F}$ to be eliminated. The FE model used soil properties as listed in Table 2 with results shown in Figure 8. The towing speeds considered are between 0.01<s<0.21 ms^{-1} which equates to a strain rate between 0.01<$\bar{\varepsilon}$<0.18

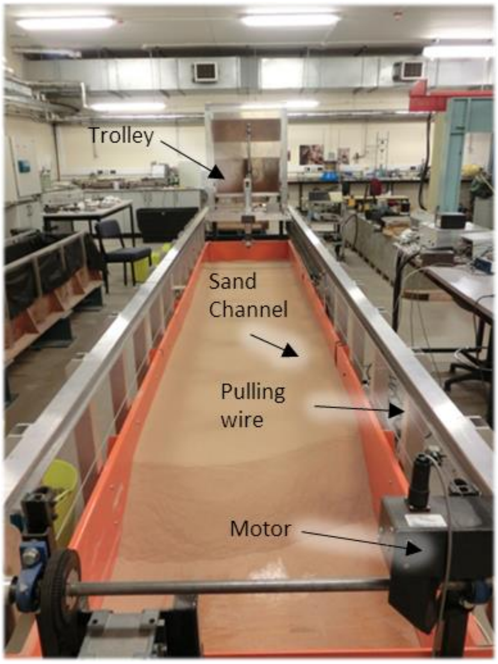

Figure 7: Laboratory setup to measure drag force of discs on soil (from Casanovas-Revilla [37])

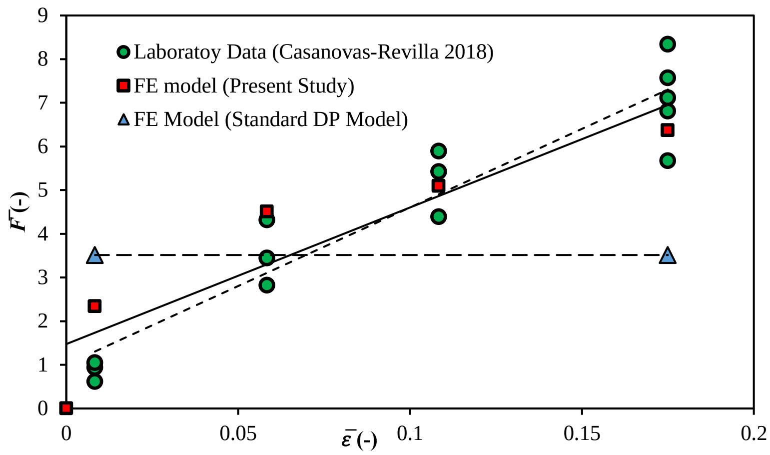

Figure 8: $\bar{F}$ vs $\bar{\varepsilon}$ for disc with *d*=0.12m and *t*=0.09m and fixed *z*=0.009m

The standard DP model displays no sensitivity to towing speed as the there are no post yield effects within the soil. The rate-dependent DP model, however, allows for increasing elastic deformation with increasing strain rates, and shows good correlation with the experimental data. Although the FE model overpredicts $\bar{F}$ at $\bar{\varepsilon}$ < 0.07, it shows good correlation with the lower bound of the experimental data at $\bar{\varepsilon}$ > 0.07. At $\bar{\varepsilon}$ < 0.07 the resultant shear strength in the model is relatively low, which causes instability in the DP model. This effect has been documented previously [20] and is countered in Abaqus/Explicit by injecting viscous damping into the model which results in increased stiffness and thus increased drag force [36]. The formation of the frontal and lateral berm in front of the moving geometry partially embedded in the seabed can be seen in Figure 9.

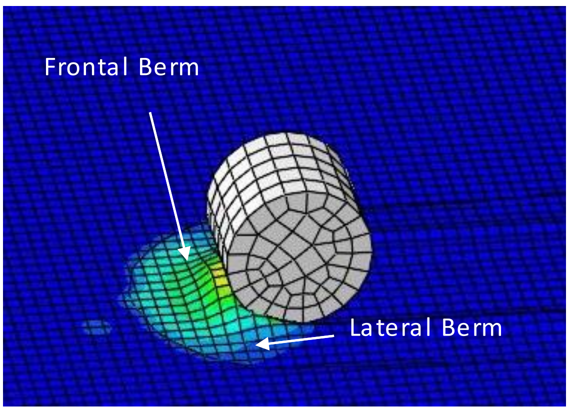

Figure 9 :Fully developed frontal and lateral berm during horizontal motion of single disc (*d*=0.2 m, *t*=0.15 m)

The estimated strain rate, $\dot{\varepsilon}$, (where $\dot{\varepsilon} = d/s$) is dimensional whereas the strain rate observed in the FE model $\dot{\varepsilon}_{FE}$, is the maximum strain rate across the 3 principal dimensions and can accurately determine the yield strength of each mesh element. It is also noted that the effect of *s* is non-linear, as the shear strength of the soil is a logarithmic function which reaches a limit state after $\dot{\varepsilon}_{FE}$ > 10. It is this ability to predict the magnitude of strain rate across 3 dimensions in the contact area that allows the increase in shear strength in saturated soil to be determined accurately using the FE model. The limiting strain rate, $\dot{\varepsilon}_{limit}$, represents a strain rate above which the generation of negative pore pressure reaches a maximum and cannot increase the effective stress state of the soil. For this study, $\dot{\varepsilon}_{limit}$=10 s^{-1} and is chosen since experimental observations showed the increment in shear strength to be minimal beyond this value. This property will be dependent on the soil properties (primarily grain sizing and permeability) and will vary accordingly, though will be valid for coarse grained sands similar to those used in this study.

3.2. Validation with Sea Trials

O'Neill et al [9] measured the drag force acting on truncated non-rolling discs during experimental trials at sea, which are compared here with predictions from the FE model. In the sea trials, rigid discs of different sizes and with aspect ratios in the range 0.75<*t/d* <1.5, were fitted to a benthic sledge via an axle and a supporting framework. The supporting framework was free to move in the vertical direction, and hence, the vertical forces that the discs exerted on the seabed were the gravitational forces of the axle, framework and discs. An illustration of this arrangement is shown in

Figure 10 (b) while the a schematic view is presented in

Figure 10 (a) . It was possible to increase the applied vertical force by attaching weights to the framework and each disc was tested at three different weights while the XY loadcell was able to measure the horizontal drag force on the discs. The towing speed was increased incrementally over a 30 min period during each deployment from 1 to 2 ms^{-1}, and the forces acting on the discs were measured continuously. The sediment was sandy and had an average d_{50} of 0.10 mm and a 12% silt and clay components compared to the coarser sand soil with a d_{50} of 0.17 mm used in the FE model.

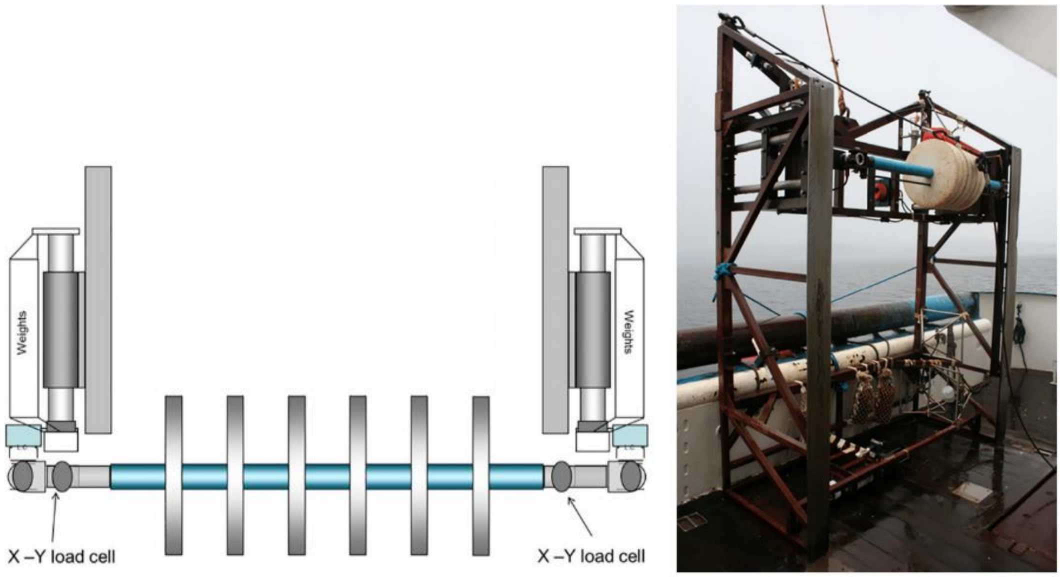

(a) **(b)**

Figure 10: Schematic of multiple disc arrangement used to measure drag force during sea trials (a) and the towed framework (sitting upright) used to tow the discs across the seabed [9]

3.2.1. Single Disc

Generally, there is good correlation between the FE model and experimental data (Figure 11). Some discrepancies are observed at W=1764 N, where the experimental observations, which are only obtained for a small range of $\bar{\varepsilon}$ (0.7 < $\bar{\varepsilon}$< 0.9), show a high degree of scatter, although the magnitudes of $\bar{F}$ are comparable. This result is postulated to be due to the effect of tidal current on the vessel which led to the inability to maintain the lower bound of speed ($\bar{\varepsilon}$ = 0.6) and would also then effect the hydrodynamic lift applied to the sledge, in turn affecting the accuracy of the experimental data. In all cases, the trends of $\bar{F}$ varying with $\bar{\varepsilon}$ are seen to correspond well, with $\bar{F}$ decreasing with increasing $\bar{\varepsilon}$. This appears contrary to the fixed penetration models discussed previously but is due to a reduction in $\bar{z}$ with increasing $\bar{\varepsilon}$. This is driven by the increase in effective stress state in the shear zone beneath the disc due to the increased strain rate in the soil, causing a reduction in penetration.

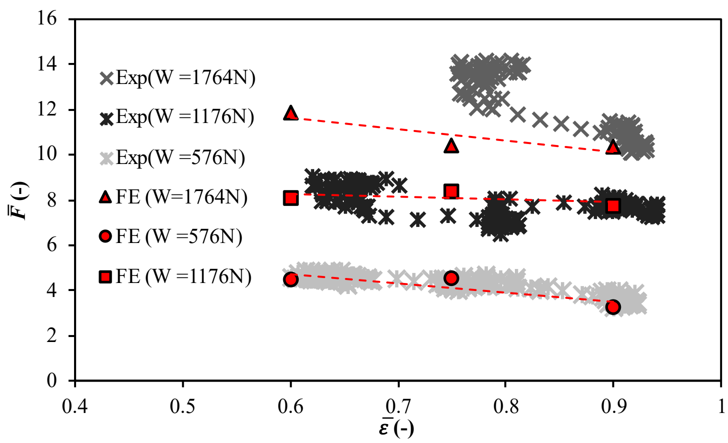

Figure 11: Comparisons with sea-trials for $\bar{F}$ against $\bar{\varepsilon}$ for single disc of *d*=0.2 m *t*=0.15 m

This is seen clearly in Figure 12 where the effect of $\bar{\varepsilon}$ on $\bar{z}$ is observed for various values of $\bar{W}$. At $\bar{W}$ = 13.13 (W=1764 N), the decrease in $\bar{z}$ is seen to be relatively high, decreasing from $\bar{z}$=0.13 to $\bar{z}$=0.07 as $\bar{\varepsilon}$ tends to 1.0. However, at $\bar{W}$ = 8.75 (W=1176 N) and $\bar{W}$ =4.23 (W=576 N), the decrease in $\bar{z}$ is relatively minor due to a smaller initial contact area and a smaller volume of displaced soil. In all cases $\bar{z}$ approaches a steady state as $\bar{\varepsilon}$ approaches 1 due to the displaced soil approaching an undrained state where no further increases in shear strength are seen. Magnitudes of z observed in this data set were between 6-24 mm and are within the ranges seen in previous studies [7] [8]. It is concluded that the variation of $\bar{z}$ with $\bar{\varepsilon}$ has a significant effect on resultant $\bar{F}$. The effect of aspect ratio t/d has also been considered as an additional sensitivity which has shown no appreciable difference in $\bar{F}$ when 0.75 < t/d < 2.0. Observations made in [37] also indicated at t/d > 1.5 no change in $\bar{F}$ was seen.

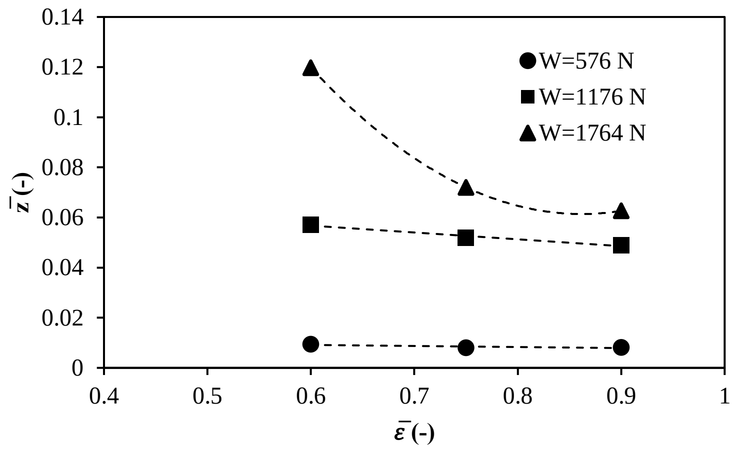

Figure 12: $\bar{\varepsilon}$ vs $\bar{z}$ for varying *W* for single disc *t*= 0.2m and *d*=0.15m

The discrepancies between the FE model and sea trials in the measured drag force at higher $\bar{W}$ are primarily due to the non-homogenous soil in the seabed where the sea trials were conducted. In-situ sieving analysis conducted show a significantly higher proportion of finer particles and has a d_{10} of 0.045 mm compared to the d_{10} of 0.17 mm for granular soil used in the FE model. This adversely affects the accuracy of the FE model as the DP model used is intended to describe purely granular soil and cannot account for the non-homogenous soil seen in the sea-trials. The difference in d_{10} also affects the permeability of the soil and in turn affects its rate-dependant shear strength. This effect is more significant at higher $\bar{W}$ as this deforms a greater volume of soil owing to higher penetration and magnifies the error in the constitutive model.

3.2.2. Multiple Disc

Comparisons with a multiple disc geometry are presented in this section. Multiple disc geometries are representative of the rockhoppers used in towed fishing gears. The deformation of the soil in front of each disc is similar to that of a single disc, however the lateral berms formed interact with each other in the spacing between the discs and this interaction depends on the spacing itself. The non-dimensional parameters for $\bar{F}$ and $\bar{W}$ are modified to account for the number of discs, *n*, in each geometry as follows:

$$\bar{F}_n = \frac{F_D}{n\gamma t d^2} \qquad \bar{W}_n = \frac{W}{n\gamma t d^2}$$

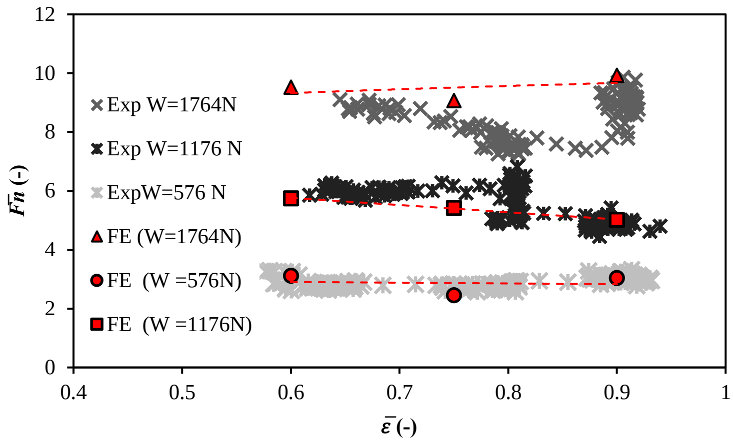

Figure 13: Experimental correlations for $\bar{F}_n$ against $\bar{\varepsilon}$ for multiple discs of *d*=0.2 m, *t*=0.025 m and *n*=6

Results from the FE Model are compared with experimental data in Figure 13 and show good correlation with observations from sea trials. This geometry is comparable to the single disc with a similar diameter and contact area. Although the contact area of the rockhopper equals that of the single disc (*ndt*=0.03 m^2), the spread of the contact patches across the geometry results in lower overall bearing pressure per disc and thus lower penetration due to self-weight (prior to horizontal motion).

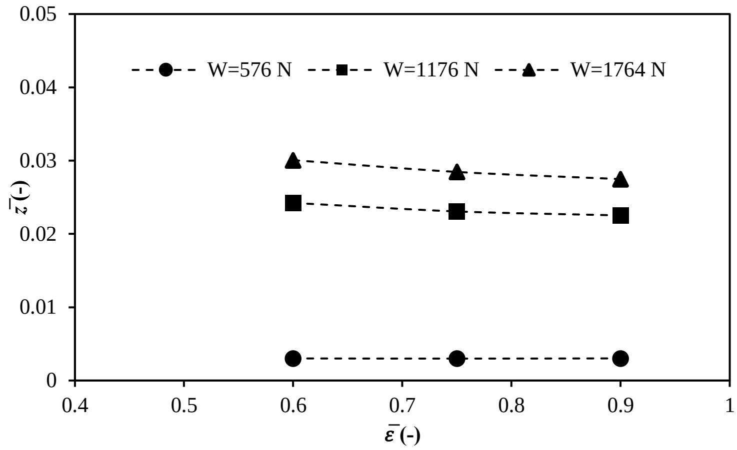

Figure 14: $\bar{\varepsilon}$ vs $\bar{z}$ for varying *W* for multiple discs of *d*=0.2 m, *t*=0.025 m and *n*=6

As a result, observations of $\bar{F}_n$ show low levels of variation with $\bar{\varepsilon}$, compared to the single disc model. For the cases of *W*=576 N and *W*=1176 N the variation of $\bar{F}_n$ with $\dot{\varepsilon}$ is seen to be minimal and corelates well with FE model results. For the case where *W*=1764 N, the experimental observations of the variation of F_D with $\bar{\varepsilon}$ are inconclusive with a reduction of $\bar{F}_n$ observed while 0.6<$\bar{\varepsilon}$<0.8 but then peaking at $\bar{\varepsilon}$ =0.9. The experimental observations for this case are affected adversely by the environmental conditions experienced during sea trials. The FE model results show only an increase in $\bar{F}_n$ with $\bar{\varepsilon}$ but compare well with the observed magnitudes. A linear regression of the experimental results also shows a similar positive trend to that observed with the FE model. The effect of $\bar{\varepsilon}$ on $\bar{z}$ is also minimal, with a minor decrease of $\bar{z}$ observed at *W*=1764 N while the lower weights showed no appreciable effect due to $\bar{\varepsilon}$ (Figure 12). This is principally due to the increased strain rates observed in the soil while being deformed by the passage of multiple discs. While $0.6<\bar{\varepsilon}<0.9$, observations of $\dot{\varepsilon}_{FE}$ indicate a majority of the soil being displaced is in a fully undrained state and presents no further increase in shear strength with increasing $\dot{\varepsilon}$. As such, there will be relatively low variation of $\bar{z}$ and resultant $\bar{F}_n$ with $\bar{\varepsilon}$, as has been observed.

4. General Observations of Strain-rate

The influence of strain rate on the soil is the primary focus of this study and is able to provide an understanding of the effect of strain rate on shear strength. The evolution of strain rate around a disc of $\bar{W}$=8.75 moving horizontally across the soil is shown in Figure 15. It is immediately visible that the majority of the soil is at resting state with a minimal strain rate and associated deformation. The increase in observed strain rate $\dot{\varepsilon}_{FE}$ is localised in the shear zone directly in front of and beneath the disc where the maximum volume of soil is displaced. When compared to the calculated strain rate ($\dot{\varepsilon}= s/d$), $\dot{\varepsilon}_{FE}$ displays significantly higher observed strain-rates. Figure 15 (a) illustrates a maximum $\dot{\varepsilon}_{FE}$ =37 s^{-1} whereas as the calculated strain rate is $\dot{\varepsilon}$=9 s^{-1}, an increase of a factor of 4 ($\dot{\varepsilon}_{FE,max} \approx 4\cdot \dot{\varepsilon}_{\max}$) with similar increase in $\dot{\varepsilon}_{FE}$ is seen in Figure 15 (b) as well. This indicates the soil has reached its maximum shear strength due to the generation of negative pore pressure and is limited by the undrained condition generated at the increased towing speed ($\dot{\varepsilon}$=9 s^{-1}). Comparisons of the soil deformation in Figure 15 (a) and (b) show the increase in strain rate seen at higher towing speeds. This leads to the increase in effective stress within the soil under deformation leading to an increase in $\bar{F}$.

However, the increase in strain rate is relatively higher beneath the disc and causes a reduction of $\bar{z}$ at higher $\dot{\varepsilon}$, which in turn leads to an increased sensitivity of $\bar{F}$ to $\dot{\varepsilon}$. This reduction in $\bar{z}$ has been documented in previous studies [37] [39], which suggested a reduction in penetration of a moving disc with increasing friction angle of a soil. As a result, the single disc geometry is significantly influenced by strain rate owing to the towing speed, especially at higher $\bar{W}$, which does require the use of a strain rate dependent constitutive model to accurately describe its behaviour.

The evolution of strain rate for a rockhopper geometry is presented in Figure 16. From the top-down view presented in Figure 16 (a) it is clear that a large area of the seabed is subject to increased strain-rates due to the greater deformation imposed. The interaction of the lateral berms formed by each disc causes areas of high strain rate between the discs along with the frontal berms observed with the single disc model. Overall, observations of $\dot{\varepsilon}_{FE}$ for a multiple disc geometry are higher ($\dot{\varepsilon}_{FE,max}$ =50 s^{-1}) when compared to a single disc of equal diameter and equivalent combined width (where $\bar{W} = \bar{W}_n$) although the calculated value remains the same where $\dot{\varepsilon}$ =9 s^{-1}.

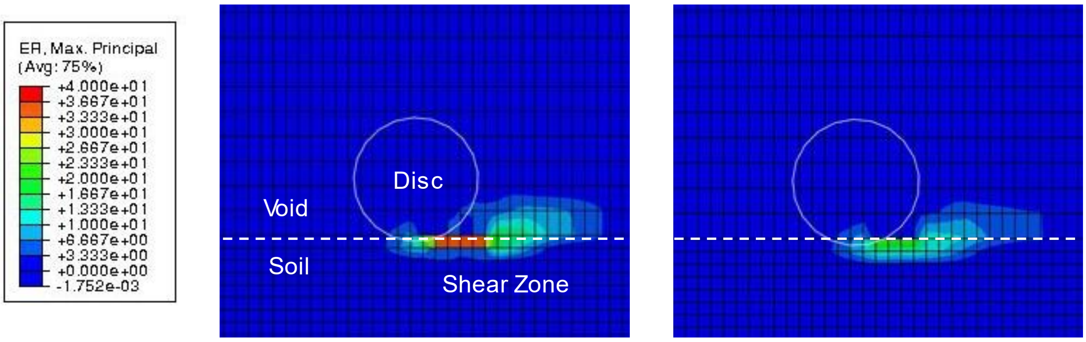

(a) (b)

Figure 15: Evolution of $\dot{\varepsilon}_{FE}$ for cross sectional cut through a single disc of d=0.2 m, at (a) $\dot{\varepsilon}$ = 9 s-1 and (b) $\dot{\varepsilon}$ = 6 s-1

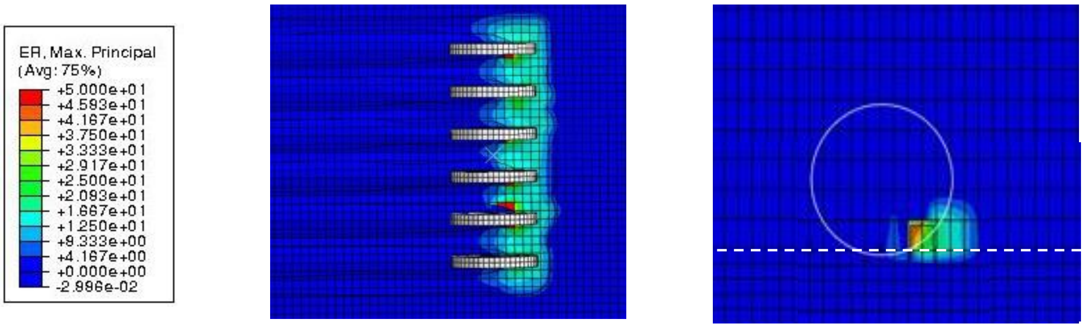

(a) (b)

Figure 16: Evolution of $\dot{\varepsilon}_{FE}$ for multiple discs of d=0.2, t=0.025 m and $\dot{\varepsilon}$ = 9 s-1 viewed from (a) a top-down view in the XY plane and (b) a cross-sectional cut in the YZ plane

This suggests that the multiple disc geometry will induce a higher strain rate in the soil compared to a comparable single disc model and will typically result in a higher effective stress state of the soil. However, since a majority of the displaced soil is subject to strain rates above the limit state, $\dot{\varepsilon}_{limit}$, it can also be surmised that $\dot{\varepsilon}$ will have a smaller effect on $\overline{F}_n$ since the soil will not continue to undergo increases in shear strength. In general terms, observations of strain rate are found to be in the range 0< $\dot{\varepsilon}_{FE}$<100, which coincides with the transition from drained to an undrained state observed experimentally. These observations enable a better understanding of the mechanics between towed fishing gears and can account for the effect of towing speed on drag force seen. In combination these findings are significant and are novel additions to this field of study.

5. Conclusion

The use of FE modelling with ABAQUS/Explicit using CEL meshing has been shown to be able to simulate the interaction between a non-rolling disc and the seabed. In addition, the use of a rate-dependent DP soil model has been shown to be able to replicate the effect of towing speeds on drag force along with the resultant penetration into seabed under dynamic conditions. Comparisons to sea-trials revealed generally good correlation and the ability to identify trends of drag force against speed for given cylindrical geometries. Although no direct comparison of penetration was available, the small-scale validation of the FE model carried out showed accurate prediction of the magnitude of drag force for a given penetration. Furthermore, as simulated drag force showed good correlation with sea-trials, it can be postulated that the penetration obtained from the FE model is valid. The discrepancies observed between FE model and sea-trials were attributed to the simplified assumptions made in the FE model regarding the seabed topology and soil type. Comparisons against literature were also seen to closely mirror observed trends [20] [37] , adding further confidence to the model. The single-phase model presented has shown to perform well for modelling transient shallow penetration problems where effects such as consolidation are less significant. The relationship between ϕ'/ϕ'_{ref} presented is only valid for granular soils with similar d_{10} size and permeability. In order to apply this model to a granular soil with differing permeability, the above relationship would have to be determined experimentally. Furthermore, it is noted that the model presented does not extend to mud or clay which have their own unique constitutive models.

The modelling methodology presented also allow for more complex geometries such as otter doors and as rotating discs to be simulated. This would allow for all components of the groundgear to be modelled discretely, allowing for geotechnical drag force and penetration to be obtained. Applying these in conjunction with correlations for angle of attack and disc spacing would then allow for drag force for an entire groundgear system to be calculated. The rate dependent constitutive model demonstrated can also be extended to varying types of soils provided a relationship between strain rate and shear strength can be determined. Finally, the modelling approaches presented could be applied to subsea trenching and ploughing where an accurate estimate of the forces involved along with the seabed deformation are required.

6. Acknowledgements

FGONs contribution was partly funded by : Grant PID2019-107345RB-I00 of the European Maritime and Fisheries Fund (EMFF) and the Ministry of Environment and Food of Denmark in the project ’Quantifying and reducing the physical impact of mobile fishing gears (ReFigure)’, (Grant Agreement No 33113-B-20-176).

References

[1] T. Cashion, D. Al-Abdulrazzak, D. Belhabib, B. Derrick, E. Divovich, D. Moutopoulos, S. Noel, M. Palomares, L. C. Teh, D. Zeller and D. Pauly, “Reconstructing global marine fishing gear use: Catches and landed values by gear type and sector,” *Fisheries Research,* no. 206, pp. 57-64, 2018.

[2] H. J. Lindeboom and S. J. (. Groot, “The effects of different types of fisheries on the North Sea and Irish Sea benthic ecosystems. IMPACT-II Report.,” NETHERLANDS INSTITUTE FOR SEA RESEARCH, Texel, 1998.

[3] C. Grieve, D. C. Brady and H. Polet, “Review of habitat dependent impacts of mobile and static fishing gears that interact with the seabed,” May 2014. [Online]. Available: https://www.msc.org/global-impacts/science-series/volume-02/benthic-impacts/at_download/file. [Accessed 05 July 2017].

[4] A. Linnane, B. Ball, B. Munday, B. van Marlen, m. Bergman and R. Fonteyne, “A review of Potential Techniques to Reduce the Environmental Impact of Demersal Trawls,” *Irish Fisheries Investigations (New Series),* vol. 7, 2000.

[5] S. Jennings, J. K. Pinnegar, N. V. Polunin and K. J. Warr, “Impacts of Trawling Disturbance on the Trophic Structure of Benthic Invertebrate Communities,” *Marine Ecology Porgress Series,* vol. 213, pp. 127-142, 2001.

[6] J. P. Bridger, “Some effects of the passage of a trawl over the seabed,” in *Institution of Chartered Engineering Surveyors (ICES)*, 1970.

[7] J. F. Caddy, “Underwater Observations on Tracks of Dredges and Trawls and Some Effects of Dredging on a Scallop Ground,” *Journal of the Fisheries Research Board of Canada,* no. 30, pp. 173-180, 1973.

[8] P. Krost, M. Bernhard and W. Hukriede, “Otter trawl tracks in Kel Bay (Western Baltic) mapped by side-scan sonar,” *Meeresforschung,* no. 32, pp. 344-354, 1990.

[9] F. G. O'Neill, K. Summerbell and A. Ivanović, “The contact drag of towed demersal fishing gear components,” *Journal of Marine systems,* no. 177, pp. 39-52, 2018.

[10] G. Qiu, S. Henke and J. Grabe, “Application of a Coupled Eulerian–Lagrangian approach on geomechanical problems involving large deformations,” *Computers and Geotechnics,* no. 38, pp. 30-39, 2011.

[11] T. Hamann, G. Qiu and J. Grabe, “Application of a Coupled Eulerian-Lagrangian approach on pile installation problems under partially drained conditions,” *Computers and Geotechnics,* no. 63, pp. 279-290, 2015.

[12] F. Van den Abeele, B. Spinewine, J.-C. Ballard and R. Denis, “Advanced Finite Element Analysis to Tackle Challenging Problems in Pipeline Geotechnics,” in *SIMULIA Community Conference*, Kent, 2013.

[13] J. T. Yi, F. H. Lee, S. H. Goh, X. Y. Zhang and J.-F. Wu, “Eulerian finite element analysis of excess pore pressure generated by spudcan installation into soft clay,” *Computers and Geotechnics,* no. 42, pp. 157-170, 2012.

[14] S. Dutta, “Numerical Modelling of Large Deformation Behaviour of Offshore Risers and Pipelines in Soft Clay Seabeds,” Memorial University of Newfoundland, St'Johns, 2017.

[15] S. Dutta, B. Hawlader and R. Philips, “Numerical investigation of dynamic embedment of offshore pipelines,” in *Conference on Soil Mechanics and Geotechnical Engineering*, Paris, 2013.

[16] H. Zhou and M. F. Randolf, “Computational techniques and shear band development for cylindrical and spherical penetrometers in strain-softening clay,” *International Journal of Geomechanics ASCE,* vol. 4, no. 7, pp. 287-295, 2007.

[17] J. P. Hambleton and A. Drescher, “Modeling wheel-induced rutting in soils: Rolling,” *Journal of Terramechanics,* no. 46, pp. 35-47, 2009.

[18] A. Ivanoivć, R. D. Neilson and F. G. O'Neill, “Modelling the Physical Impact of Demersal Fishing Gears on the Seabed and Comparison with Sea Trials,” *Ocean Engineering,* vol. I, no. 38, pp. 925-933, 2011.

[19] M. Esamaeili and A. Ivanović, “Analytical and numerical modelling of non-driven disc on friction material,” *Computers and Geotechnics,* no. 68, pp. 208-215, 2015.

[20] M. Esmaeili and A. Ivanović, “Numerical modelling of bottom trawling ground gear element on the seabed,” *Ocean Engineering,* no. 91, pp. 316-32, 2014.

[21] A. C. Palmer, “Speed Effects in Cutting and Ploughing,” *Geotechnique,* no. 3, pp. 285-294, 1999.

[22] A. G. van Os and W. van Leussen, “Basic Research on Cutting Forces in Saturated Sand,” *Journal of Geotechnical Engineering,* vol. 113, no. 12, pp. 1501-1516, 1987.

[23] K. D. Lauder, M. Brown, M. Bransby and S. Gooding, “Variation of tow force with velocity during offshore ploughing in granular materials,” *Canadian Geotechnical Journal,* vol. 11, no. 49, pp. 1244-1255, 2012.

[24] K. D. Lauder, M. J. Brown, M. F. Bransby and S. Boyes, “The influence of incorporating a forecutter on the performance of offshore pipeline ploughs,” *Applied Ocean Research,* no. 39, pp. 121-130, 2013.

[25] H. G. Larew and K. Atakol, “The effect of rate of shearing on the shearing resistance of cohesionless soil,” University of Virginia, Virginia, 1967.

[26] K. L. Lee, H. B. Seed and P. Dunlop, “Effect of transient loading on the strength of sand,” in *Proceedings of the Seventh International Conference on Soil Mechanics and Foundation Engineering*, Mexico, 1969.

[27] H. B. Seed and R. Lundgren, “Investiation of the effects of transient loading on the strength and deformation characteristics of saturated soils,” *Proceedings of ASTM,* no. 54, pp. 1288-1306, 1954.

[28] J. A. Yamamuro, A. E. Abrantes and P. V. Lade, “Effect of Strain Rate on the Stress-Strain Behavior of Sand,” *Journal of geotechnical and geoenvironmental engineering,* vol. 12, no. 137, pp. 1169-1178, 2011.

[29] E. Suescun-Florez and M. Iskander, “Effect of Fast Constant Loading Rates on the Global Behaviour of Sand in Triaxial Compression,” *Geotechnical Testing Journal ,* vol. 1, no. 40, pp. 2015-2053, 2017.

[30] K. Watanabe and O. Kusakabe, “Reappraisal of loading rate effects on sand behaviour in view of seismic design for pile foundation,” *Soilds and Foundations,* vol. 2, no. 53, pp. 215-231, 2013.

[31] S. Aluwihare, “Numerical Modelling of Towed Fishing Gears on Seabed Sediment,” University of Aberdeen, Aberdeen, 2021.

[32] DSS Simulia, “Abaqus Analysis Users Manual,” 2014. [Online]. Available: http://abaqus.software.polimi.it/v6.14/books/usi/default.htm. [Accessed June 2017].

[33] LS-Dyna, “LS-Dyna Support,” 2017. [Online]. Available: http://www.dynasupport.com/faq/general/what-are-the-differences-between-implicit-and-explicit. [Accessed 03 July 2017].

[34] K. Terzaghi, Theoretical Soil Mechanics, New York: John Wiley and Sons, Inc, 1943.

[35] R. F. Craig and J. A. Knappett, Craig's Soil Mechanics, 8th ed., New York: Spon Press, 2012.

[36] Simulia, “Abaqus Analysis User's Guide,” [Online]. Available: http://abaqus.software.polimi.it/v6.14/books/usb/default.htm. [Accessed 01 06 2017].

[37] C. Casanovas-Revilla, Experimental Investigation of the Interaction of Bottom Trawled Fishing Gears and the Seabed, Aberdeen: University of Aberdeen, 2018.

[38] A. Eslami and A. Mohammadi, “Drained soil shear strength parameters from CPTu data for marine deposits by analytical model,” *Ships and Offshore Structures,* vol. 8, no. 11, pp. 913-925, 2016.

[39] M. G. Bekker, Introduction to Terrain-Vehicle Systems, Michigan: University of Michigan Press, 1969.

[40] F. G. O'Neill and K. Summerbell, “The hydrodynamic drag and the mobilisation of sediment into the water column of towed fishing gear components,” *Journal of Marine Systems,* no. 164, pp. 76-84, 2016.